Numerical Study of Passive Control of an Over-Expanded Nozzle for Fighter Aircraft

Douglas A. Terrier[1] and Frank K. Lu[2]

[1] Lockheed Martin Aeronautics Company, Fort Worth, Texas, USA
[2] University of Texas at Arlington, Arlington, Texas, USA

Abstract. An experimental and computational study showed that a passive boundary layer control device in the form of a step incorporated just downstream of a nozzle throat can be used to provide good thrust recovery. The nozzle without the step produced an overexpansion of the supersonic flow. The computational study was performed for a full-scale nozzle under actual engine exhaust and ambient atmospheric conditions. The original baseline nozzle flow was highly over-expanded, to produce an extensive region of sub-ambient pressure along almost the entire extent of the divergent region. This caused complex shock, boundary layer interactions toward the nozzle exit. When a step was added near the downstream of the nozzle throat, it reduced the over-expansion, thereby yielding a better pressure recovery in the divergent region. The computed value of thrust coefficient compared well against that of a 12 percent scale model. The data showed a 2.5 percent improvement in performance over the baseline.

1 Introduction

Recent fighter aircraft development includes thrust vectoring as an important performance feature [1]. For example, the X-35B fighter aircraft shown in Fig. 1 utilizes an advanced propulsion system to achieve short takeoff and vertical landing (STOVL). The engine is fitted with an articulated exhaust duct that allows vectoring for STOVL operation. In addition, a lift fan system is mounted just aft of the cockpit. The lift fan is powered by a mechanical drive shaft connected to the main engine through a clutch mechanism. In STOVL mode, the lift fan balances the thrust of the aft nozzle. In addition, small nozzles in each wing provide roll control. The components of the STOVL propulsion system are shown in Fig. 2.

Because of limitations in the kinematics of the engine nozzle, it is only possible to design to a few key performance points and accept the fall-out performance at other points. These key performance points that affect the survivability of the aircraft therefore drive the selection of the area ratio schedule. With a nozzle throat area $A_8 = 0.290$ m^2, the value of the nozzle exit-to-throat area ratio $A_9/A_8 = 1.2$ is selected to provide high thrust efficiency in the cruise (non afterburning) configuration. At $A_8 = 0.484$ m^2, a value of $A_9/A_8 = 1.3$ is selected to give good performance at after-burning conditions. Because the hover condition occurs at $A_8 = 0.484$ m^2, it also presents an $A_9/A_8 = 1.3$.

A 12% scale model test of the baseline nozzle design was conducted at the Lockheed Martin Aeronautics Thrust Measurement (TMF) Facility in Fort

Fig. 1. Lockheed Martin X-35B STOVL fighter aircraft

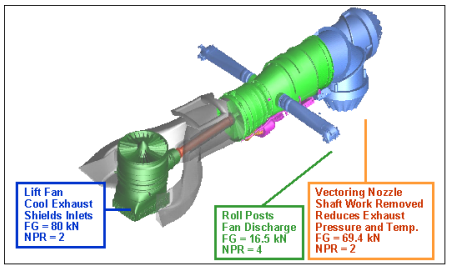

Fig. 2. X-35B STOVL propulsion system

Worth, Texas. The thrust coefficient (Cfg) results of this test for $A_8 = 0.484$ m^2 and $A_9/A_8 = 1.3$ is compared in Fig. 1 with analytical prediction of thrust performance for $A_9/A_8 = 1.3$ and $A_9/A_8 = 1.1$. This comparison reveals that the nozzle provides good performance at after-burning conditions, but exhibits significant thrust loss at hover relative to a nozzle with $A_9/A_8 = 1.1$. This thrust loss is due to over-expansion of the supersonic nozzle flow in the divergent section downstream of the throat. An aft-facing step at the nozzle throat was proposed as a passive method of inducing boundary flow separation and thereby relieving the over-expansion loss [2]. The present investigation utilizes numerical analysis to identify the design parameters and quantify the performance of the aft-facing step configuration.

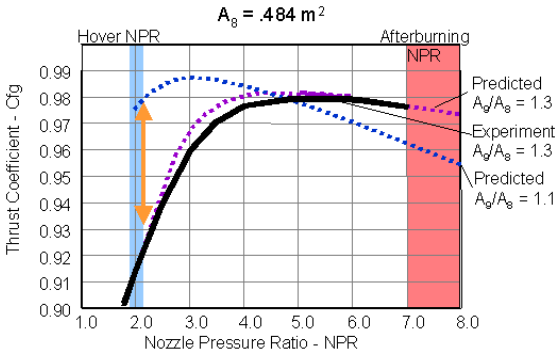

Fig. 3. X-35B baseline nozzle results, NPR = nozzle pressure ratio

2 Method

An extensive parametric analysis of the step boundary layer control design was conducted using computational fluid dynamics techniques to examine eight

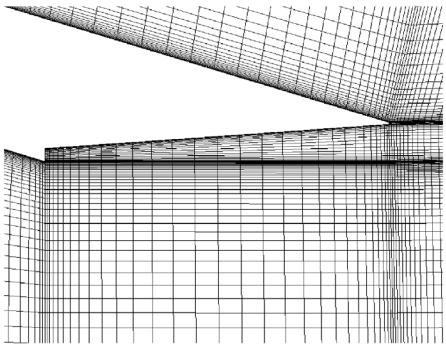

Fig. 4. CFD grid for $A_9/A_8 = 1.3$, $A_s/A_8 = 1.1$ configuration

geometry configurations at NPR's ranging from 2.0 to 8.0 for a total of 33 distinct cases. The time-averaged Navier-Stokes equations were solved using the `FALCON` code developed at Lockheed Martin in Fort Worth. `FALCON` uses a finite-volume approach on a multiple block structured grid to achieve greater conservation qualities than comparable finite-difference codes. `FALCON` includes the two-equation k-kl and k-l turbulence models as well as a large eddy simulation model for accurate turbulence calculations and a wall-layer model (or wall function) to reduce the number of points required for accurate boundary layer calculations. The code also includes the capability to solve very low speed and mixed speed flows using a technique known as low speed preconditioning. Boundary conditions can be set along any grid surface/line in the grid. Three types of interfaces between multiple blocks of grid are currently available in `FALCON`. The first assumes the grids match at the boundary point-for-point. The second is called non-point-to-point matched and only requires that an extrapolated grid point can be found in some other block. The third type is similar to the matched interfaces except that the interface data is filtered through some type of transfer function before being applied to the opposite interface patch.

In this analysis, `FALCON` was run in the axi-symmetric mode with a grid consisting of approximately 90 points in the axial direction and 40 points in the radial direction for a total of about 3,600 grid points. Eight different grid geometry configurations simulating variations on the X-35 nozzle in the hover or after-burning mode with $A_8 = 0.484$ m^2 were defined. Three nozzle expansion ratios were examined: $A_9/A_8 = 1.1$, 1.3 and 1.5. These represent the range of A_9/A_8 that could practically be considered for the X-35 application. For the $A_9/A_8 = 1.1$ case, a baseline configuration and a slot size of $A_s/A_8 = 1.1$ were run. For the $A_9/A_8 = 1.3$ and 1.5 cases, a baseline configuration, a slot size of $A_s/A_8 = 1.1$, and a slot size of $A_s/A_8 = 1.2$ were run. The detail grid structure in the region of the step is shown for the $A_9/A_8 = 1.3$, $A_s/A_8 = 1.1$ case in Fig. 4. All cases were run at full-scale geometry with a representative engine exhaust total temperature of 780 K. Inflow total pressure was specified to simulate NPR's covering the range from hover at NPR = 2.0 to supersonic after-burning acceleration at NPR = 8.0. The exit boundary condition was specified at sea level standard atmospheric conditions of $p = 101.3$ kPa and $T = 294$ K.

In order to capture the interaction of the external flow-field, the grids extend to the region outside the nozzle.

3 Results

Results of the CFD study for the baseline configuration at the hover condition are presented in Fig. 5. The local velocity vectors are represented as scaled arrows colored by pressure. Several flow features are evident in a close examination of this plot. The flow is seen to accelerate through a Prandtl-Meyer expansion from a sonic condition approaching the throat to high supersonic speed as it continues into the divergent section. The initial Prandtl-Meyer fan just downstream of the throat is governed by the divergent flap angle, and further flow expansion occurs downstream in the complex flow region due to reflected waves. Also shown in Fig. 5 is a plot of pressure along the nozzle surface. The flow is highly over-expanded, producing sub-ambient pressures along almost the entire extent of the divergent flap. This region of low pressure acting on the aft facing area of the divergent flap produces a significant drag force that is the source of the thrust loss at hover. Near the trailing edge the flow encounters an adverse pressure gradient due to the influence of the ambient pressure, resulting in a shock boundary layer separation. In the separated region the flow recovers to ambient pressure and, as a result, produces less drag. It is intuitively obvious from the baseline results that a configuration that promotes more extensive separation along the divergent flap will yield less drag and therefore higher thrust. This reveals the essential principle behind the step configurations developed in this study. Specifically, the step promotes boundary layer separation thereby reducing drag on the divergent flap.

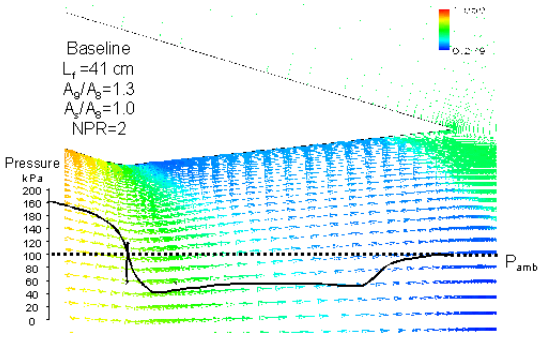

Fig. 5. CFD result for $A_9/A_8 = 1.3$, baseline nozzle, NPR=2

The CFD results for the baseline configuration at NPR = 6 representing the transonic acceleration, after-burning point are shown in Fig. 6. In this high NPR case, the flow remains at higher than ambient pressure as it expands through the divergent section of the nozzle. In contrast to the hover case the divergent flap yields positive pressure resulting in additional thrust. This illustrates the

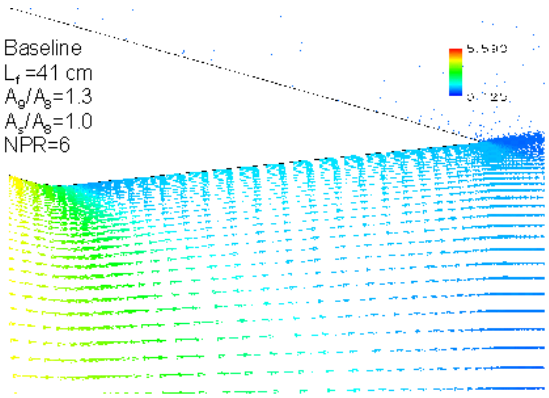

Fig. 6. CFD result for $A_9/A_8 = 1.3$, baseline nozzle, NPR=6

physical reason why this relatively large area ratio of $A_9/A_8 = 1.3$ is required to exploit the thrust potential of the flow at this condition.

The CFD results for $A_9/A_8 = 1.3$, with a step size of $A_s/A_8 = 1.1$ at the hover condition of NPR = 2.0 are shown in Fig. 7. In this case, boundary layer separation is induced by the step, and the flow is not attached to the nozzle wall. The computed flow details were similar to those found experimentally [3]. As a result, the Prandtl-Meyer expansion at the throat and over-expansion downstream is not as severe as in the baseline case. The net effect is that pressures on the divergent flap are significantly higher than in the baseline case. In the separated region between the divergent flap and the nozzle flow, a region of complex secondary flow is created. This region is acted on by shear forces at the slip line formed at the boundary of the primary flow. Close examination of Fig. 7 reveals the presence of an inflow from the external flow-field into this cavity and a region of re-circulation adjacent to the primary flow slip line. The entrained velocity in this region produces pressures that are below ambient, but still higher than the baseline case. The resulting divergent flap pressures are also plotted in Fig. 7.

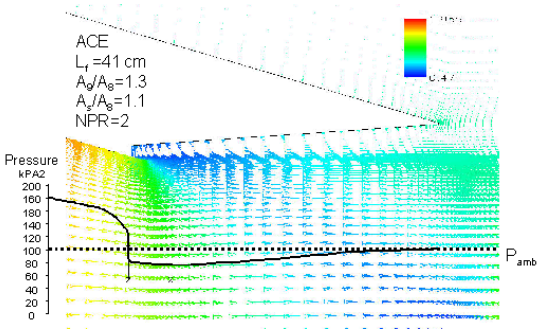

Fig. 7. CFD result for $A_9/A_8 = 1.3$, $A_s/A_8 = 1.1$, NPR=2

Figure 8 shows a comparison of the CFD pressure data on the divergent flap of the baseline and $A_s/A_8 = 1.1$ cases, both for $A_9/A_8 = 1.3$. This comparison

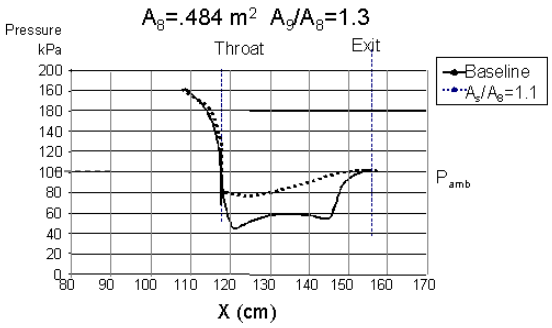

Fig. 8. Pressure comparison for baseline and $A_9/A_8 = 1.3$, $A_s/A_8 = 1.1$

clearly shows higher divergent flap pressure and therefore reduced drag resulting from the effect of the step. The region of sub-ambient pressures representing thrust loss on the divergent flap is about half that of the baseline configuration. Figure 8 illustrates the improved pressure recovery as the physical mechanism responsible for the thrust recovery potential of the step configuration.

The result for the $A_9/A_8 = 1.3$, $A_s/A_8 = 1.1$ case at the transonic acceleration condition with NPR = 6 is shown in Fig. 9. In this case, boundary layer separation is initially induced by the step causing a separated region immediately downstream of the throat. In contrast to the hover case however, the favorable pressure gradient present at this condition causes the flow to immediately reattach to the divergent flap. Above-ambient pressures are experienced along the remainder of the divergent flap resulting in good thrust performance. The limited separated region just downstream of the throat experiences sub-ambient pressures that act on the aft facing area of the step contributing to approximately 0.5% lower thrust performance than the baseline at this condition.

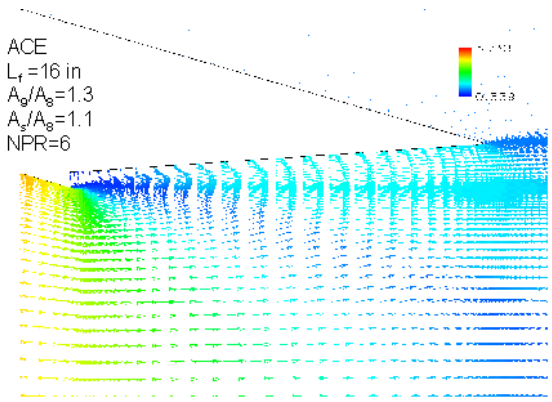

Fig. 9. CFD result for $A_9/A_8 = 1.3$, $A_s/A_8 = 1.1$, NPR=6.0

The `FALCON` code includes post-processing routines that permit convenient integration of momentum and pressure forces to give gross thrust. The thrust coefficient results for all thirty-three cases run are plotted in Fig. 10. The data show that the step is effective in inducing separation and improves hover perfor-

mance by approximately 2.5% relative to the baseline design. In addition, the NPR at which separation is induced increases with step size and A_9/A_8. The results are cross plotted to illustrate the effect of step size and A_9/A_8 on Cfg in Fig. 11 and on separation NPR in Fig. 12.

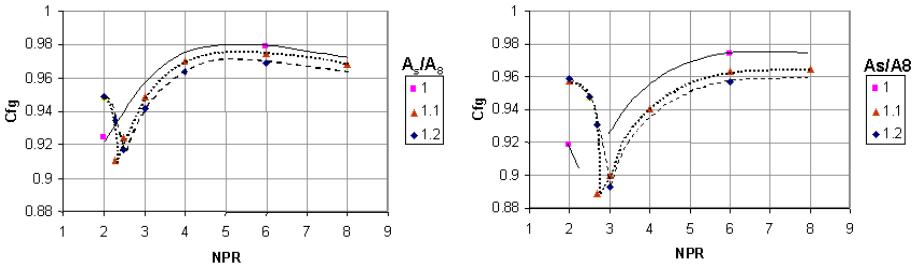

a. $A_9/A_8 = 1.3$ b. $A_9/A_8 = 1.5$

Fig. 10. CFD predictions for various nozzle configurations

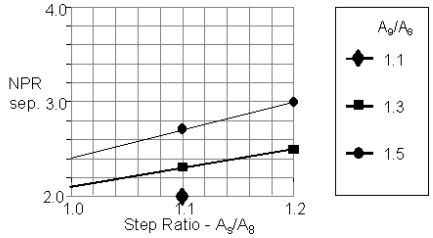

Fig. 11. CFD predictions for effect of step size on Cfg

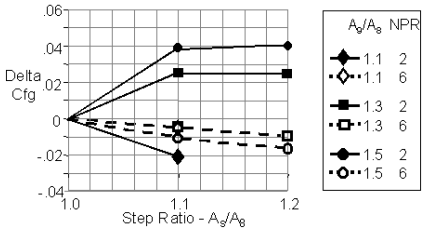

Fig. 12. CFD predictions of step size vs separation NPR

A 12% scale model test was conducted in the Lockheed Martin TMF to validate CFD predictions of the step performance. Three nozzles with $A_8 = 0.484$ m^2 and $A_9/A_8 = 1.3$ representing the baseline, a step size of 1.1 and a step size of $A_s/A_8 = 1.2$ were tested. The test data for the baseline and step size of 1.1 are compared with CFD predictions in Fig. 13. The predictions and test data compare very well at all conditions with a maximum difference of less than 0.5%. This plot dramatically demonstrates the improvement of approximately 2.5% in Cfg at the hover condition due to the $A_s/A_8 = 1.1$ step. The test results fully verify the CFD analysis and verify the performance of the step configuration. Preliminary mechanical studies as shown in Fig. 14 have shown that this step can be incorporated in the nozzle structure with minimal impact in cost and weight.

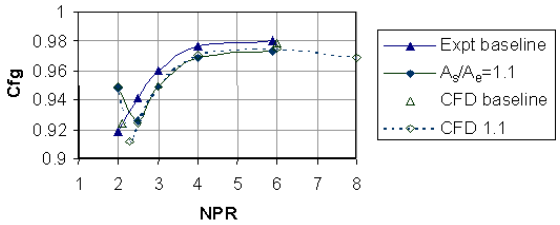

Fig. 13. Comparison of CFD predictions with $A_s/A_8 = 1.1$ and baseline test ($A_8 = 0.484$ m^2, $A_9/A_8 = 1.3$)

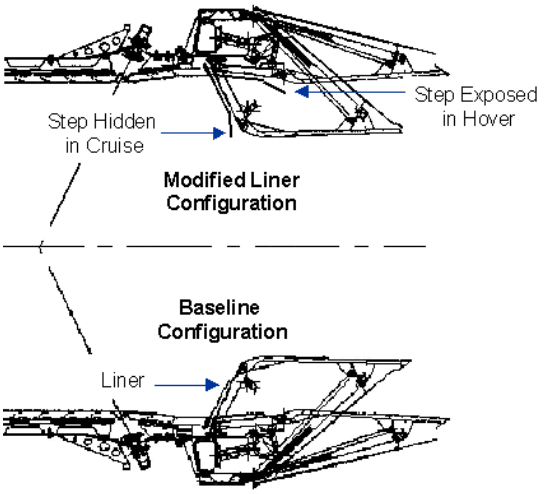

Fig. 14. Preliminary mechanical design of step concept

4 Conclusions

The concept featuring a passive boundary layer control step provides a thrust increase of approximately 2.5% relative to the baseline at the X-35 hover condition. The design parameters and performance predictions for the step configuration were developed using CFD analysis and verified through sub-scale model testing. This study defines the fundamental geometry parameters for a successful step concept, and provides preliminary designs for incorporating the concept in the X-35 nozzle. In addition, the extensive CFD analysis matrix yields results that may be generalized to other over-expanded internal transonic flows.

References

1. Berens TM, Bissinger NC (1998) Thrust vector behavior of highly integrated asymmetric nozzles for advanced fighter aircraft. AIAA 98–0948
2. Samimy M, Petrie HL, Addy AL (1986) A study of compressible turbulent reattaching free shear layers. AIAA J 24:261–267
3. Hama FR (1968) Experimental studies on the lip shock. AIAA J 6(2):212–219